INTERNATIONAL JOURNAL FOR NUMERICAL METHODS IN FLUIDS
Int. J. Numer. Meth. Fluids 2003; **43**:1–23 (DOI: 10.1002/fld.595)

An accurate and efficient finite-difference algorithm for non-hydrostatic free-surface flow with application to wave propagation

G. Stelling[1,*,†] and M. Zijlema[1,2]

[1] *Fluid Mechanics Section, Faculty of Civil Engineering and Geosciences, Delft University of Technology, Stevinweg 1, 2628 CN Delft, The Netherlands*
[2] *National Institute for Coastal and Marine Management/RIKZ, P.O. Box 20907, 2500 EX The Hague, The Netherlands*

SUMMARY

A numerical technique is presented for the approximation of vertical gradient of the non-hydrostatic pressure arising in the Reynolds-averaged Navier–Stokes equations for simulating non-hydrostatic free-surface flows. It is based on the Keller-box method that take into account the effect of non-hydrostatic pressure with a very small number of vertical grid points. As a result, the proposed technique is capable of simulating relatively short wave propagation, where both frequency dispersion and non-linear effects play an important role, in an accurate and efficient manner. Numerical examples are provided to illustrate this; accurate wave characteristics are already achieved with only two layers. Copyright © 2003 John Wiley & Sons, Ltd.

KEY WORDS: free-surface flow; non-hydrostatic pressure; Keller-box scheme; wave propagation

1. INTRODUCTION

The design of efficient and accurate numerical algorithms is an essential prerequisite for the simulation of wave propagation from deep water through the surf zone, particularly for coastal engineering-type applications. Boussinesq-type wave equations with improved dispersion characteristics formulated by, e.g. Madsen and Sørensen [1] and Nwogu [2] are well suited to model different wave phenomena, especially in shallow water regions, such as non-linearity, dispersion and shoaling. Also, these models include implicitly refraction and diffraction. Since, the Boussinesq-type wave models are based on an efficient depth-integrated formulation, they also have become very popular for real-life applications involving wave dynamics in coastal regions and harbours. However, a well-known drawback of the Boussinesq-type modelling is

*Correspondence to: G. Stelling, Fluid Mechanics Section, Faculty of Civil Engineering and Geosciences, Delft University of Technology, Stevinweg 1, 2628 CN Delft, The Netherlands.
† E-mail:g.stelling@ct.tudelft.nl

Received 26 May 2002
Revised 14 April 2003

the assumption of an irrotational and inviscid flow. As a consequence, neither the interaction of waves with rotational currents nor the effects of viscosity on the wave motion can be simulated.

An alternative route is a numerical solution for incompressible turbulent fluid flows involving gravity waves based on the time-dependent three-dimensional Reynolds-averaged Navier–Stokes equations. This approach is not only suitable to model wave-dominated flows over the entire range of water depths but also for simulating wave disturbance in real fluid with rotation and shear. A number of studies have been reported in which the features of this approach in the context of wave dynamics have been investigated.

In the papers of Casulli and Stelling [3], Casulli [4] and Stelling and Busnelli [5], a fractional step method is proposed that describes the inclusion of non-hydrostatic pressure by solving a Poisson equation in the hydrostatic free-surface flow model of Casulli and Cheng [6]. This hydrostatic model solves the three-dimensional (3D) shallow water equations in Cartesian co-ordinates whereby the vertical accelerations are neglected and the vertical velocity is obtained from the (local) continuity equation. Such a model is sufficiently accurate for large-scale flow phenomena like tidal and wind-driven flows in coastal seas, lakes, estuaries and rivers, but prohibits a correct calculation of short surface waves. The underlying motivation for the proposed fractional step approach is that the existing shallow water solver needs not to be adapted, since the correction to the hydrostatic pressure is done after the shallow water equations have been solved. As a consequence, this reduced the effort of software maintenance to a minimum. Moreover, Mahadevan *et al.* [7] have shown that this technique also leads to a more stable and efficient non-hydrostatic calculations than in a case without splitting the pressure into hydrostatic and non-hydrostatic parts. An example of the latter procedure can be found in Mayer *et al.* [8], where two-dimensional (2D) Euler equations including total pressure is solved and the surface elevation is determined by means of a kinematic boundary condition along the free surface.

The method of decomposing the pressure into hydrostatic and non-hydrostatic components has also been employed by Stansby and Zhou [9] and Zhou and Stansby [10]. However, their method is formulated in the sigma co-ordinate system, except for the horizontal non-hydrostatic pressure gradient which is retained in Cartesian co-ordinates since, sigma transformation of the horizontal gradients may introduce large truncation errors near a steep bed resulting from the summation of large terms of opposite sign [11]. These truncation errors can cause spurious flows. Like Casulli and Stelling [3], a conjugate gradient method is employed for the solution of Poisson pressure equation. In the former paper, they also demonstrated the use of their model for simulating waves and currents over trenches and hills. A similar procedure is discussed by Li and Fleming [12]. They discretized the momentum equations with McCormack's explicit scheme that is restricted by the CFL stability condition related to the gravity wave speed. Furthermore, the Poisson equation for the non-hydrostatic pressure is solved by means of a multigrid technique.

It is recognized that sufficiently large number of vertical grid points is required in a 3D free-surface Navier–Stokes computation for describing wave dispersion characteristics up to an acceptable level of accuracy. In practice, this number is about 10–20, see, for instance, References [4, 10, 12, 13]. Combined with the solution of the elliptic equation for the non-hydrostatic pressure, this greatly increases the computational effort that may hamper three-dimensional applications with a sufficiently fine grid.

In this paper, we present an accurate approximation of vertical gradient of the non-hydrostatic pressure based on the Keller-box or Preissmann scheme; see, e.g. Reference [14].

This scheme is edge based with respect to the pressure whereas most other methods, such as [3–5], are cell centred. The scheme of this paper is also referred to as a Hermitian or spline method, see, e.g. Reference [15]. Due to the fact that the scheme is edge based in the vertical direction, the zero pressure boundary condition at the free surface can be approximated very accurately. In fact, it is a discrete analogue of the Boussinesq-type of wave models; the vertical dependency of the non-hydrostatic pressure can be considered to be resolved by a finite series of spline functions. The splines are described by the pressure itself and its vertical derivative. In this manner, the implicit scheme calculates the vertical gradients of the non-hydrostatic pressure at different vertical grid points simultaneously. The results presented in this paper show that this procedure allows a very small number of layers (in the order of 1–3) for the accurate simulation of relatively short waves. Even in the case of one layer, i.e. the depth-averaged mode, it predicts the frequency dispersion for fairly short waves in shallow water with an accuracy similar to that of the Boussinesq-type wave model of Peregrine [16]. For the cell centred methods this is impossible. This is due to the fact that a zero non-hydrostatic pressure in the centre of the surface cell approximates the zero pressure boundary condition at the free surface, see Reference [4]. A one-layer approximation is therefore always a hydrostatic approximation.

2. GOVERNING EQUATIONS AND BOUNDARY CONDITIONS

The computational modelling of non-hydrostatic free-surface flows with gravity waves amounts to the solution of the three-dimensional unsteady incompressible Reynolds-averaged Navier–Stokes equations. Since, we restrict ourselves to the application to the wave propagation only, we consider the 3D Euler equations. Extension to the turbulent case including Coriolis and baroclinic effects is straightforward; see, for instance, Reference [5].

We consider a physical domain that is bounded vertically by the free surface $z = \zeta(x, y, t)$ (this excludes overtopping waves) and the bottom $z = -\mathrm{d}(x, y)$; see Figure 1.

The dependent variables of the Euler equations are the velocity components u, v and w in x-, y- and z-direction, respectively, and the pressure p normalized through division by a

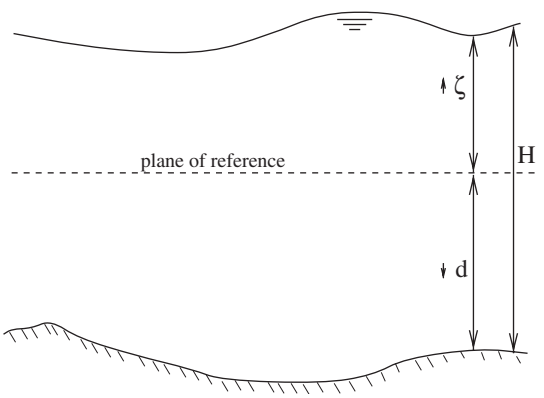

Figure 1. Water area with bottom and free surface.

constant reference density. By means of a decomposition of the pressure into a hydrostatic part p_h, assuming zero atmospheric pressure, and a non-hydrostatic part q, as follows:

$$p = g(\zeta - z) + q = p_h + q \tag{1}$$

With g the acceleration of gravity, the momentum equations are given by

$$\begin{aligned} \frac{\partial u}{\partial t} + u\frac{\partial u}{\partial x} + v\frac{\partial u}{\partial y} + w\frac{\partial u}{\partial z} + g\frac{\partial \zeta}{\partial x} + \frac{\partial q}{\partial x} &= 0 \\ \frac{\partial v}{\partial t} + u\frac{\partial v}{\partial x} + v\frac{\partial v}{\partial y} + w\frac{\partial v}{\partial z} + g\frac{\partial \zeta}{\partial y} + \frac{\partial q}{\partial y} &= 0 \\ \frac{\partial w}{\partial t} + u\frac{\partial w}{\partial x} + v\frac{\partial w}{\partial y} + w\frac{\partial w}{\partial z} + \frac{\partial q}{\partial z} &= 0 \end{aligned} \tag{2}$$

Note that the hydrostatic balance as given by

$$\frac{\partial p_h}{\partial z} = -g \tag{3}$$

is subtracted out in the equation for vertical velocity (2). Due to incompressibility, the momentum equations (2) must be solved together with the (local) continuity equation:

$$\frac{\partial u}{\partial x} + \frac{\partial v}{\partial y} + \frac{\partial w}{\partial z} = 0 \tag{4}$$

Since, we are dealing with the free-surface flows we need an extra equation for the determination of water level ζ. By means of integration of the continuity equation (4) over the water depth $H = \zeta + d$, and subsequent the use of the Leibniz' rule and insertion of the kinematic conditions, which are given by

$$\begin{aligned} w|_{z=\zeta} &= \frac{\partial \zeta}{\partial t} + u\frac{\partial \zeta}{\partial x} + v\frac{\partial \zeta}{\partial y} \\ w|_{z=-d} &= -u\frac{\partial d}{\partial x} - v\frac{\partial d}{\partial y} \end{aligned} \tag{5}$$

We obtain the so-called free-surface condition:

$$\frac{\partial \zeta}{\partial t} + \frac{\partial}{\partial x}\int_{-d}^{\zeta} u\,\mathrm{d}z + \frac{\partial}{\partial y}\int_{-d}^{\zeta} v\,\mathrm{d}z = 0 \tag{6}$$

Boundary conditions are required at all the boundaries of a three-dimensional domain including the bottom and the free surface. Only one normal and two tangential components of the velocities and/or stresses need to be described at the boundaries in order to get a unique solution.

At the free surface, the continuity of normal and tangential stresses is enforced [17]. Since we consider the Euler equations, the specification of two tangential stresses, i.e. wind stresses, is superfluous. Hence, we have the following Dirichlet boundary condition for the total pressure:

$$-p|_{z=\zeta} = 2\frac{\gamma}{R} \tag{7}$$

where γ is the surface tension, R is the radius of curvature of the surface. Note that in (7) both the viscous stress and atmospheric pressure have been neglected. In the motion of gravity waves, which is our interest, the surface tension can be ignored. By virtue of (1), we have

$$q|_{z=\zeta} = 0 \tag{8}$$

At the bottom, the normal component of the velocity, i.e. w-velocity, is imposed according to the kinematic condition at the bottom (5). Moreover, two tangential stresses are usually specified by means of the bottom stresses, which are neglected in this case.

At inflow, an incident normal wave velocity component obtained from linear wave theory, is specified by

$$\mathbf{u} \cdot \mathbf{n}|_{\text{inflow}} = \frac{\omega a}{kH} f_{\text{r}} \sin \omega t \tag{9}$$

with a the wave amplitude, $\omega = 2\pi/T$ the angular frequency of the wave with T the wave period, $k = 2\pi/l$ the wave number with l the wavelength, and

$$f_{\text{r}}(t) = \frac{1}{2}\left(1 + \tanh \frac{t - 3T}{T}\right) \tag{10}$$

the so-called ramp-function that is used to prevent initially short waves with relatively large amplitudes. Furthermore, tangential velocity components are set to zero. It should be noted that no boundary conditions for both water level and non-hydrostatic pressure component are required since, no momentum equation for the normal velocity is solved at the inflow boundary.

At outflow, absorbing boundary conditions are employed by means of a sponge layer technique. For this, the computational domain is extended, for instance in x-direction, with a sponge layer sizing a multiple of wavelength. No use of a Sommerfeld-type radiation condition is made for the test cases considered in this study. It should be noted, however, that the use of sponge layer technique might not be efficient as compared to the use of radiation condition. Nevertheless, the test cases show that the use of the below described sponge layer approach is to be very effective in wave absorption. The following sponge layer formula of Reference [17] is used:

$$v = \begin{cases} \dfrac{1}{4}\left(\tanh\left[\dfrac{\sin(\pi(4\tilde{x} - 1)/2)}{1 - (4\tilde{x} - 1)^2}\right] + 1\right), & 0 < \tilde{x} < \dfrac{1}{2} \\ \dfrac{1}{4}\left(\tanh\left[\dfrac{\sin(\pi(3 - 4\tilde{x})/2)}{1 - (3 - 4\tilde{x})^2}\right] + 1\right), & \dfrac{1}{2} < \tilde{x} < 1 \end{cases} \tag{11}$$

with $\tilde{x} = (x - L_0)/L$, where L denotes the length of the sponge layer which starts at $x = L_0$, and v is a damping coefficient of a linear damping term added to the u-momentum equation, as follows:

$$\frac{\partial u}{\partial t} + \cdots + vu = 0 \tag{12}$$

Outside the sponge layer, $v \equiv 0$. Note that the damping coefficient v is not only vanishing at the leading edge of the sponge layer but also at the trailing edge in order not to alter the propagation characteristics of the outgoing waves. At the end of the extended domain,

the water level, the non-hydrostatic component of pressure and the normal gradient for the tangential components of the velocity are set to zero. Note that the normal velocity component is computed from the free-surface condition (6).

At closed boundaries, fully reflective or free-slip conditions are applied, i.e. the velocity normal to the wall is zero, whereas a zero normal gradient for the tangential velocity components is specified. For the case of a vertical wall parallel to y-axis, these conditions are thus given by

$$u = \frac{\partial v}{\partial x} = \frac{\partial w}{\partial x} = 0 \tag{13}$$

3. DISCRETIZED EQUATIONS AND SOLUTION METHOD

The numerical models often cover areas where the bathymetry is irregular. Moreover, the free surface varies as a function of time. In practice, the sigma co-ordinate system and a Cartesian framework are suitable candidates for the sufficiently accurate discretization of the governing equations in the vertical direction (see, e.g. References [6, 10]). For the sake of transparency, however, we present our approach formulated in the Cartesian co-ordinates, although it can be described in the sigma co-ordinates as well. As a consequence, the immobile bottom is represented as a staircase. At the free surface, a drying-and-flooding algorithm allows the free surface to move freely through the vertical grid. Depending on this algorithm, the number of active grid layers may be function of time and space.

We introduce a set of strictly horizontal levels

$$\{z_{k-1/2} \,|\, k = 1, \ldots, K+1 \wedge \forall (x,y)\colon\ z_{1/2} \leqslant -d(x,y) \leqslant \zeta(x,y,t) \leqslant z_{K+1/2}\} \tag{14}$$

and a horizontal grid defined by

$$\{\mathbf{x} \,|\, x_{i-1/2} = (i-1)\Delta x,\ y_{j-1/2} = (j-1)\Delta y, i = 1, \ldots, I+1, j = 1, \ldots, J+1\} \tag{15}$$

A three-dimensional cell with centre at (x_i, y_j, z_k) is bounded by the intersection of the water column between the bottom and the free surface with the horizontal levels $z_{k\pm1/2}$ and the horizontal grid lines $x_{i\pm1/2}$ and $y_{j\pm1/2}$. The length Δx and the width Δy of the cell are not necessarily equal to each other. The layer thickness of the cell is defined as

$$\Delta z_k^n = \min[\zeta_{i,j}^n, z_{k+1/2}] - \max[-d_{i,j}, z_{k-1/2}] \tag{16}$$

with n denoting the present time level. A cell is wet as long as $\Delta z_k^n > 0$. The number of wet cells in the water column for point (x_i, y_j) depends on the position of the free surface and the bottom. The vertical index of the cell at the free surface is denoted as $k_{\text{top}}(i,j)$, whereas the cell just above the bottom is denoted as $k_{\text{bottom}}(i,j)$.

A staggered grid arrangement is employed, in which the velocity components u, v and w are located at the centre of the cell faces $(i+1/2, j, k)$, $(i, j+1/2, k)$ and $(i, j, k+1/2)$, respectively. Contrary to what is usual, the non-hydrostatic pressure component q is given at the faces $(i, j, k+1/2)$ rather than at the cell centres (i, j, k), because of the application of the Keller-box scheme to be presented. Figure 2 shows the arrangement of the unknowns.

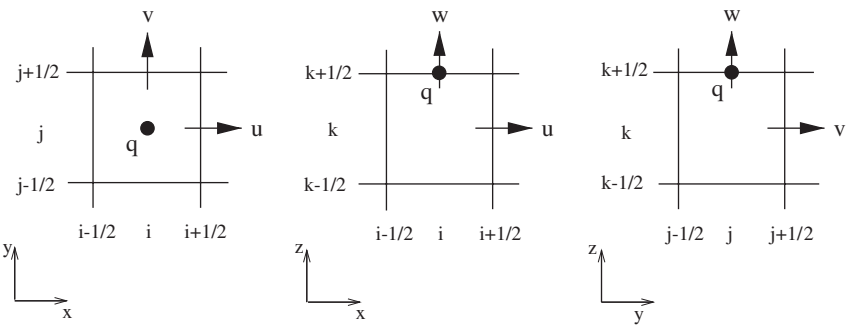

Figure 2. Arrangement of the unknowns in a staggered grid.

The wet layer thickness of both surface and bottom layer at a velocity point is not uniquely defined. In the present implementation, we used a so-called 'upwind' approach. To this end, the depth-averaged velocities are employed, as given by

$$U^{n+1}_{i+1/2,j} = \frac{1}{H^n_{i+1/2,j}} \sum_{k=k_{\text{bottom}}}^{k_{\text{top}}} u^{n+1}_{i+1/2,j,k} \Delta z^n_k, \quad V^{n+1}_{i,j+1/2} = \frac{1}{H^n_{i,j+1/2}} \sum_{k=k_{\text{bottom}}}^{k_{\text{top}}} v^{n+1}_{i,j+1/2,k} \Delta z^n_k \tag{17}$$

with $H^n_{i+1/2,j}$ and $H^n_{i,j+1/2}$ the total depths at points $(i+1/2,j)$ and $(i,j+1/2)$, respectively.

The layer thickness of both surface and bottom layer at, for instance, u-velocity point $(i+1/2,j)$ depends on the direction of $U_{i+1/2,j}$, as follows:

$$\Delta z^{n,U}_{k_{\text{top}}} = \begin{cases} \zeta^n_{i,j} - z_{k_{\text{top}}-1} & \text{if } U^n_{i+1/2,j} > 0 \\ \zeta^n_{i+1,j} - z_{k_{\text{top}}-1} & \text{if } U^n_{i+1/2,j} < 0 \\ \max(\zeta^n_{i,j}, \zeta^n_{i+1,j}) - z_{k_{\text{top}}-1} & \text{if } U^n_{i+1/2,j} = 0 \end{cases} \tag{18}$$

and

$$\Delta z^{n,U}_{k_{\text{bottom}}} = \begin{cases} z_{k_{\text{bottom}}+1} + d_{i,j} & \text{if } U^n_{i+1/2,j} > 0 \\ z_{k_{\text{bottom}}+1} + d_{i+1,j} & \text{if } U^n_{i+1/2,j} < 0 \\ z_{k_{\text{bottom}}+1} + \min(d_{i,j}, d_{i+1,j}) & \text{if } U^n_{i+1/2,j} = 0 \end{cases} \tag{19}$$

This upwind approach guarantees a positive total water depth in the water level points.

For the outline of the discretization of the governing equations as presented in Section 2, we distinguish between the multi-layer case and the case with a single layer. These are described in Sections 3.1 and 3.2, respectively. The discretization for the single-layer case is treated separately, since its evaluation can be done in a very efficient manner. For the sake of clarity, the horizontal momentum equations will be discretized by means of a second-order explicit finite-difference technique. Although, this imposes the time-step limit through the CFL condition for long surface waves, it was not restrictive for the test cases presented in this paper. Nevertheless, the present approach can be applied in an implicit framework similar to that of Casulli and Stelling [3] as well. The vertical momentum equation is discretized with

the Keller-box scheme. This scheme allows a very few number of vertical grid points, without deteriorating the accuracy of the frequency dispersion for relative short waves. The objective of this paper is to show that even for relative complicated wave propagation over uneven bottoms, high accuracy of the corresponding wave characteristics is already achieved with only two layers. With respect to time discretization of both horizontal and vertical momentum equations, any higher-order scheme can be used. Here, we adopted the well-known leapfrog scheme due its simplicity and accuracy for propagation problems for relative short waves with respect to the number of grid points per wavelength.

3.1. Numerical approximation for the multi-layer case

In this section, we describe the numerical method for the multi-layer case, i.e. $K>1$. Space discretization of the governing equations is carried out in the usual way, except for the vertical momentum equation. The discretization of this equation is based upon the Keller-box scheme, as follows:

$$\begin{aligned}
&\frac{w^{n+1}_{i,j,k+1/2}-w^{n}_{i,j,k+1/2}+w^{n+1}_{i,j,k-1/2}-w^{n}_{i,j,k-1/2}}{2\Delta t}\\
&\quad+\frac{1}{2}\left(\overline{u^{n}_{i,j,k+1/2}}^{zx}(L_x w^n)_{i,j,k+1/2}+\overline{u^{n}_{i,j,k-1/2}}^{zx}(L_x w^n)_{i,j,k-1/2}\right)\\
&\quad+\frac{1}{2}\left(\overline{v^{n}_{i,j,k+1/2}}^{zy}(L_y w^n)_{i,j,k+1/2}+\overline{v^{n}_{i,j,k-1/2}}^{zy}(L_y w^n)_{i,j,k-1/2}\right)\\
&\quad+\frac{1}{2}\left(w^{n}_{i,j,k+1/2}(L_z w^n)_{i,j,k+1/2}+w^{n}_{i,j,k-1/2}(L_z w^n)_{i,j,k-1/2}\right)\\
&\quad+\frac{q^{n+1}_{i,j,k+1/2}-q^{n+1}_{i,j,k-1/2}}{\Delta z^n_k}=0
\end{aligned}\tag{20}$$

where the over bar notation is used to denote averages, for instance,

$$\overline{u}^{zx}_{i,j,k+1/2}=\tfrac{1}{4}\left(u_{i+1/2,j,k}+u_{i-1/2,j,k}+u_{i+1/2,j,k+1}+u_{i-1/2,j,k+1}\right)\tag{21}$$

With respect to the finite-difference operators L_x, L_y and L_z for the explicit approximation of the advection terms, any appropriate difference scheme can be employed. Here, a momentum conservative scheme following Stelling and Busnelli [5] is used and will not be given here. This scheme is developed for simulating shallow water flows with large gradients. Conservation of momentum is the most important aspect near local flow discontinuities in case of steep bottom gradients, hydraulic jumps or breaking waves.

Discretization of the continuity equation (4) gives

$$\Delta z^n_k\left(\frac{u^{n+1}_{i+1/2,j,k}-u^{n+1}_{i-1/2,j,k}}{\Delta x}+\frac{v^{n+1}_{i,j+1/2,k}-v^{n+1}_{i,j-1/2,k}}{\Delta y}\right)+w^{n+1}_{i,j,k+1/2}-w^{n+1}_{i,j,k-1/2}=0\tag{22}$$

The horizontal momentum equations (2) are discretized as follows:

$$\begin{aligned}&\frac{u^{n+1}_{i+1/2,j,k}-u^{n}_{i+1/2,j,k}}{\Delta t}\\&\quad+u^{n}_{i+1/2,j,k}(L_x u^n)_{i+1/2,j,k}+\overline{v^n}^{xy}_{i+1/2,j,k}(L_y u^n)_{i+1/2,j,k}+\overline{w^n}^{xz}_{i+1/2,j,k}(L_z u^n)_{i+1/2,j,k}\\&\quad+g\,\frac{\zeta^n_{i+1,j,k}-\zeta^n_{i,j,k}}{\Delta x}+\frac{q^{n+1}_{i+1,j,k+1/2}-q^{n+1}_{i,j,k+1/2}+q^{n+1}_{i+1,j,k-1/2}-q^{n+1}_{i,j,k-1/2}}{2\Delta x}=0\end{aligned}\tag{23}$$

and

$$\begin{aligned}&\frac{v^{n+1}_{i,j+1/2,k}-v^{n}_{i,j+1/2,k}}{\Delta t}\\&\quad+\overline{u^n}^{yx}_{i,j+1/2,k}(L_x v^n)_{i,j+1/2,k}+v^{n}_{i,j+1/2,k}(L_y v^n)_{i,j+1/2,k}+\overline{w^n}^{yz}_{i,j+1/2,k}(L_z v^n)_{i,j+1/2,k}\\&\quad+g\,\frac{\zeta^n_{i,j+1,k}-\zeta^n_{i,j,k}}{\Delta y}+\frac{q^{n+1}_{i,j+1,k+1/2}-q^{n+1}_{i,j,k+1/2}+q^{n+1}_{i,j+1,k-1/2}-q^{n+1}_{i,j,k-1/2}}{2\Delta y}=0\end{aligned}\tag{24}$$

Discretization of the free-surface condition (6) is obtained as follows:

$$\frac{\zeta^{n+1}_{i,j}-\zeta^n_{i,j}}{\Delta t}+\frac{H^n_{i+1/2,j}U^{n+1}_{i+1/2,j}-H^n_{i-1/2,j}U^{n+1}_{i-1/2,j}}{\Delta x}+\frac{H^n_{i,j+1/2}V^{n+1}_{i,j+1/2}-H^n_{i,j-1/2}V^{n+1}_{i,j-1/2}}{\Delta y}=0\tag{25}$$

Finally, a discretization for the kinematic condition at the free surface takes the following form:

$$\begin{aligned}w^{n+1}_{i,j,k_{\mathrm{top}}}=&\frac{\zeta^{n+1}_{i,j}-\zeta^n_{i,j}}{\Delta t}+\max(0,u^{n+1}_{i-1/2,j,k_{\mathrm{top}}})\frac{\zeta^n_{i,j}-\zeta^n_{i-1,j}}{\Delta x}+\min(0,u^{n+1}_{i+1/2,j,k_{\mathrm{top}}})\frac{\zeta^n_{i+1,j}-\zeta^n_{i,j}}{\Delta x}\\&+\max(0,v^{n+1}_{i,j-1/2,k_{\mathrm{top}}})\frac{\zeta^n_{i,j}-\zeta^n_{i,j-1}}{\Delta y}+\min(0,v^{n+1}_{i,j+1/2,k_{\mathrm{top}}})\frac{\zeta^n_{i,j+1}-\zeta^n_{i,j}}{\Delta y}\end{aligned}\tag{26}$$

whereas at the bottom, we have

$$\begin{aligned}w^{n+1}_{i,j,k_{\mathrm{bottom}}}=&-\max(0,u^{n+1}_{i-1/2,j,k_{\mathrm{bottom}}})\frac{d_{i,j}-d_{i-1,j}}{\Delta x}-\min(0,u^{n+1}_{i+1/2,j,k_{\mathrm{bottom}}})\frac{d_{i+1,j}-d_{i,j}}{\Delta x}\\&-\max(0,v^{n+1}_{i,j-1/2,k_{\mathrm{bottom}}})\frac{d_{i,j}-d_{i,j-1}}{\Delta y}-\min(0,v^{n+1}_{i,j+1/2,k_{\mathrm{bottom}}})\frac{d_{i,j+1}-d_{i,j}}{\Delta y}\end{aligned}\tag{27}$$

In order to update the unknowns of Equations (20)–(27), the sequence of the computation is as follows:

1. Substitute Equation (27) into Equations (20) and (22).

2. Starting at level $k = k_{\text{bottom}} + 1$, substitute Equation (20) corresponding to level $k - 1/2$ into Equation (20) corresponding to level $k + 1/2$ and repeat this until the level $k = k_{\text{top}}$ is reached. In this way, the explicit expression for $w_{i,j,k+1/2}$ for each level $k + 1/2$ is achieved.
3. Thereafter, Equations (23), (24) and the just evaluated vertical velocities are substituted into Equation (22). We obtained a linear system of equations for q^{n+1} that can be regarded as a discretized form of the Poisson equation. Contrary to the method presented by, for instance, Casulli and Stelling [3], this resulting system of equations is not symmetric and not positive definite even when the Cartesian system is employed. Note that $q^{n+1}_{k_{\text{top}}} = 0$ along the free surface.
4. The obtained system with unknowns q^{n+1} is solved efficiently using the Bi-CGSTAB solver with an ILU-type preconditioner. Further details on this solver and preconditioner can be found in References [18, 19], respectively.
5. Compute u^{n+1} by substitution of q^{n+1} into Equation (23).
6. Compute v^{n+1} by substitution of q^{n+1} into Equation (24).
7. Compute w^{n+1} by substitution of q^{n+1} into Equation (20).
8. Compute ζ^{n+1} by substitution of w^{n+1} into Equation (26) or alternatively from Equation (25).

3.2. Numerical approximation for the case with a single layer

This section concerns with the numerical approximation for the case with a single layer. Due to the edge-based approach, with the zero pressure boundary condition exactly at the free surface this is possible. It may be comparable to a Boussinesq-type wave model. In essence, this approach is similar to the one described in the previous section. Without losing generality and because of the test cases with a single layer considered in this paper, we restrict ourselves to a 2DV framework with one horizontal direction, say x, and vertical direction. The depth-averaged velocity U is employed and the arrangement of this variable, vertical velocity w, water level ζ and non-hydrostatic pressure component q in staggered grid is displayed in Figure 3.

The depth-averaged momentum equation is derived by means of integration of the u-momentum equation (2) over the water depth H. Writing in the non-conservative form, this yields

$$\frac{\partial U}{\partial t} + U\frac{\partial U}{\partial x} + g\frac{\partial \zeta}{\partial x} + \frac{1}{H}\int_{-d}^{\zeta}\frac{\partial q}{\partial x}\,\mathrm{d}z = 0 \tag{28}$$

Note that the vertical advection term is vanished due to the kinematic conditions (5). Special attention is paid to the vertical integration of the non-hydrostatic pressure gradient in (28). By virtue of the Leibniz' rule and (8), we have

$$\int_{-d}^{\zeta}\frac{\partial q}{\partial x}\,\mathrm{d}z = \frac{\partial}{\partial x}\int_{-d}^{\zeta} q\,\mathrm{d}z - q|_{z=-d}\frac{\partial d}{\partial x} \tag{29}$$

The integral as occurred in the right-hand side of (29) is approximated by

$$\int_{-d}^{\zeta} q\,\mathrm{d}z \approx \frac{1}{2}H(q|_{z=\zeta} + q|_{z=-d}) = \frac{1}{2}Hq|_{z=-d} \tag{30}$$

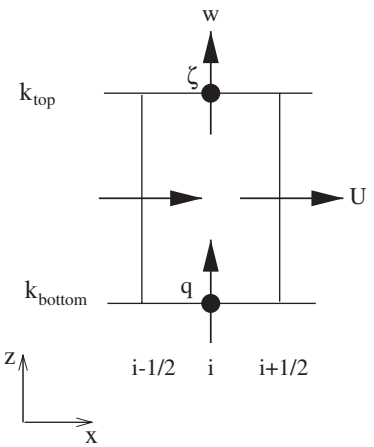

Figure 3. Grid stencil for the depth-averaged case.

Finally, writing (29) in the non-conservative form, we obtain

$$\int_{-d}^{\zeta} \frac{\partial q}{\partial x}\,\mathrm{d}z = \frac{1}{2} H \frac{\partial q|_{z=-d}}{\partial x} + \frac{1}{2} q|_{z=-d} \frac{\partial(\zeta - d)}{\partial x} \tag{31}$$

Discretization of the depth-averaged momentum equation (28) at point $i + 1/2$ gives

$$\begin{aligned} &\frac{U_{i+1/2}^{n+1} - U_{i+1/2}^{n}}{\Delta t} + U_{i+1/2}^{n}(L_x U^n)_{i+1/2} + g \frac{\zeta_{i+1}^{n} - \zeta_i^{n}}{\Delta x} \\ &\quad + \frac{q_{i+1}^{n+1} - q_i^{n+1}}{2\Delta x} + \frac{\overline{q^{n+1}}^{x}{}_{i+1/2}}{H_{i+1/2}^{n}} \frac{\zeta_{i+1}^{n} - \zeta_i^{n} - d_{i+1} + d_i}{2\Delta x} = 0 \end{aligned} \tag{32}$$

Since, q at the free surface is zero we only consider q at the bottom, therefore we have dropped the vertical index of q.

The vertical momentum equation is discretized using the Keller-box scheme:

$$\frac{w_{i,k_{\mathrm{top}}}^{n+1} - w_{i,k_{\mathrm{top}}}^{n} + w_{i,k_{\mathrm{bottom}}}^{n+1} - w_{i,k_{\mathrm{bottom}}}^{n}}{2\Delta t} + \frac{1}{2}\overline{u_i^n}^{x}((L_x w^n)_{i,k_{\mathrm{top}}} + (L_x w^n)_{i,k_{\mathrm{bottom}}}) - \frac{q_i^{n+1}}{H_i^n} = 0 \tag{33}$$

with H_i^n defined at a water level point. The discretized form of the continuity equation (4) becomes

$$H_i^n \frac{U_{i+1/2}^{n+1} - U_{i-1/2}^{n+1}}{\Delta x} + w_{i,k_{\mathrm{top}}}^{n+1} - w_{i,k_{\mathrm{bottom}}}^{n+1} = 0 \tag{34}$$

Discretization of the kinematic condition at the free surface leads to

$$w_{i,k_{\text{top}}}^{n+1} = \frac{\zeta_i^{n+1} - \zeta_i^n}{\Delta t} + \max(0, U_{i-1/2}^{n+1}) \frac{\zeta_i^n - \zeta_{i-1}^n}{\Delta x} + \min(0, U_{i+1/2}^{n+1}) \frac{\zeta_{i+1}^n - \zeta_i^n}{\Delta x} \tag{35}$$

and at the bottom, we have

$$w_{i,k_{\text{bottom}}}^{n+1} = -\max(0, U_{i-1/2}^{n+1}) \frac{d_i - d_{i-1}}{\Delta x} - \min(0, U_{i+1/2}^{n+1}) \frac{d_{i+1} - d_i}{\Delta x} \tag{36}$$

The computational procedure is now as follows:

1. Substitute Equation (36) into Equations (33) and (34).
2. Substitute Equations (32) and (33) into Equation (34), yielding a tridiagonal system of equations for q^{n+1} (or a pentadiagonal system for a 2DH case).
3. Solve the tridiagonal system for q^{n+1} by means of Gaussian elimination (or cyclic reduction in case of 2DH).
4. Compute U^{n+1} by substitution of q^{n+1} into Equation (32).
5. Compute $w_{k_{\text{bottom}}}^{n+1}$ by means of Equation (36).
6. Compute $w_{k_{\text{top}}}^{n+1}$ by substitution of q^{n+1} and $w_{k_{\text{bottom}}}^{n+1}$ into Equation (33).
7. Compute ζ^{n+1} using Equation (35).

4. NUMERICAL EXPERIMENTS

The properties of the proposed method have been evaluated by considering four test cases concerning short waves for which either analytic solutions or experimental data exist. In all cases the bottom friction and viscosity are set to zero.

The first test case is a standing short wave in a 2DV closed basin where the length and the depth of the basin are of the same order. For these dimensions, vertical accelerations can no longer be neglected. This test case was used by different authors like Casulli and Stelling [3], Mayer *et al*. [8], Casulli [4] and Chen [20]. The main objective of simulating this test case is to explore the accuracy of the proposed method in case of modelling the linear wave dispersion.

The second test case is a solitary wave, as used by Weilbeer and Jankowski [21] and Namin *et al*. [22], which should preserve its shape for the non-hydrostatic case.

In the third test case, the propagation of regular waves over a submerged bar, as described in References [23, 24], is considered. This case has been frequently employed for the evaluation of the performance of various Boussinesq-type models; see, e.g. Reference [25]. Most of these models described well the shoaling process on the upward slope of the bar. However, due to the relative steepness of the lee side of the bar, differences in the dispersion between these models are discerned. Therefore, by means of this test case the accuracy of the proposed method with respect to the shoaling process as well as the linear dispersion is examined.

Finally, the fourth test case concerns the wave deformation by an elliptic shoal resting on a plane slope, where wave change in lateral direction occurs due to refraction. With this test case provided with experimental data, we thus verify the ability of the present model to simulate this phenomenon but also diffraction and wave focussing.

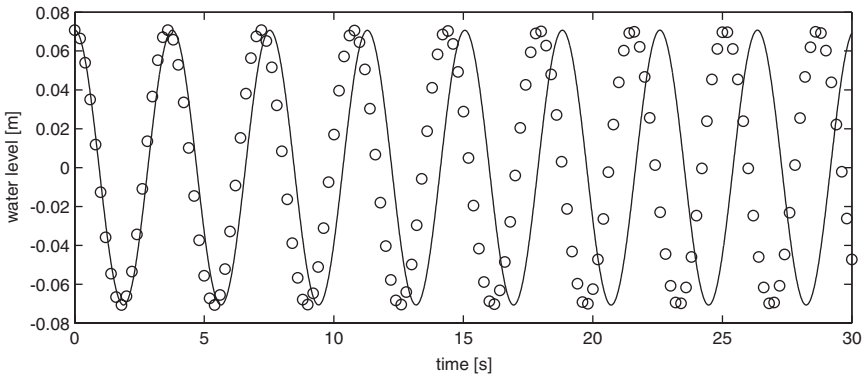

Figure 4. Comparison between computed (one layer) and exact time series of surface elevation at $x = 17.5$ m for the standing wave in closed basin. Present method (solid line), exact (circles).

4.1. *Standing short wave in closed basin*

We consider a standing wave in a closed basin with length of 20 m and depth of 10 m. Initially, the following wave height is taken:

$$\zeta = a \cos\left(\frac{\pi x}{10}\right), \quad 0 \leqslant x \leqslant 20 \tag{37}$$

where a is the amplitude of the standing wave. Here, the wavelength equals the length of the basin. For sufficiently small a, the propagation speed of the wave c is specified by the following (linear) dispersion relation:

$$c = \frac{\omega}{k} = \sqrt{\frac{g}{k} \tanh(kH)} \tag{38}$$

In our example, we choose $a = 0.1$ m. Since $kH = \pi > 1$, the wave is highly dispersive. According to formula (38), we expect that the wave period $T = 3.59$ s.

For the simulation of the seiching of the closed basin, it is divided horizontally into 20 grid cells of each 1 m, while the depth consists of a number of layers to be specified later. The time step is taken as 0.1 s.

First, a computation is performed with a single layer. In Figure 4, the time series of the computed surface elevation obtained with one layer and the exact solution obtained from linear wave theory are compared at $x = 17.5$ m.

The computed wave period of $T = 3.79$ s is clearly not correct. Apparently, the model with one layer predicts the wave celerity in deep water erroneously. It seems that, for one layer, the non-hydrostatic part in (2) are of $O(\mu^2)$, with $\mu = kH$, indicating the relative importance of linear dispersion. This means that this model using one layer approximate at most the lowest-order effect of linear wave dispersion like the standard Boussinesq-type model of Peregrine [16], i.e. it is valid for $\mu < 1$.

To improve the accuracy of the model in case of the deep-water limit, more than one layer should be employed in the calculation, which enables to resolve the hyperbolic vertical

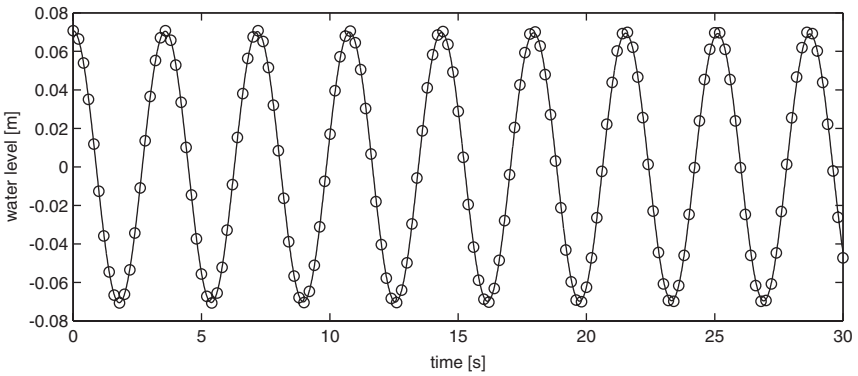

Figure 5. Comparison between computed (two layers) and exact time series of surface elevation at $x = 17.5$ m for the standing wave in closed basin. Present method (solid line), exact (circles).

velocity profile. Hence, the simulation is repeated with two layers and the result including the comparison with the analytical one is shown in Figure 5. Clearly, the computed frequency of the wave is improved and equals the exact one. It is to be stressed here that we just need only two layers to obtain the already accurate dispersion relation (38), due to the use of the Keller-box scheme that allows non-hydrostatic pressure also in the surface cells.

The above-mentioned test case was also computed by Casulli and Stelling [3]. They employed a simple approximation of the vertical pressure gradient (similar to the horizontal counterpart) and 20 layers, resulting in a good agreement with the analytical result (38). Another point of discussion is that, contrary to our results, their computed waves are damped during their propagation. This is not caused by the vertical space discretization but by the splitting error of $O(\Delta t)$ introduced in the fractional step approach that they have employed, as is shown by Casulli [4]. He is using a modified fractional step method where the splitting error is almost completely eliminated. The spatial discretization of this method however still requires hydrostatic pressure in the surface cell. The present approach with the Keller-box scheme also in the surface cells yields even more accurate waves, in which the amplitude is hardly changed.

4.2. Solitary wave in channel

The second test case is the propagation of a solitary wave in a long channel. This test case was also simulated by Weilbeer and Jankowski [21] by means of a non-hydrostatic finite-element flow model and Namin *et al.* [22] with a different kind of non-hydrostatic flow model. The solitary wave is a non-linear wave of finite amplitude, which is not a solution of the shallow water equations. Characteristic of the solitary wave is that it is neither preceded nor followed by any free-surface disturbance. Since, bottom friction and viscosity are absent, the solitary wave must travel over a horizontal bottom without changing its shape and velocity. The accuracy of the proposed numerical method for this type of wave problems can be evaluated by comparing the solution with the analytical one for an infinitely long 2DV channel. Let a be the wave height, d the mean water depth and $c = \sqrt{g(d+a)}$ the wave celerity. The water

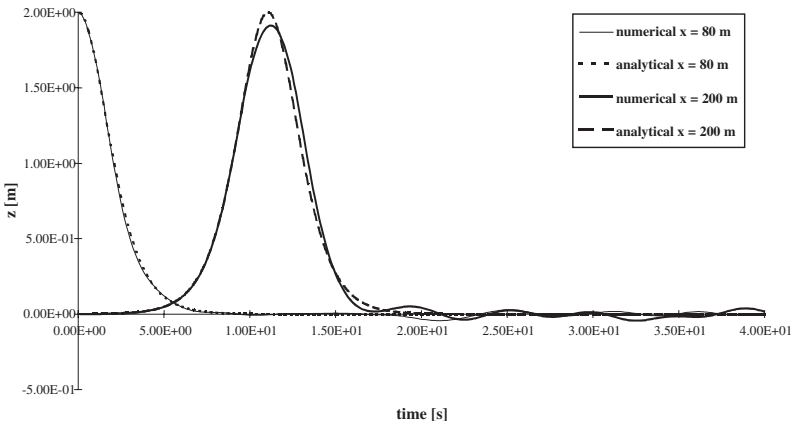

Figure 6. Comparison between computed and exact time series of surface elevation at $x = 80$ and 200 m for the solitary wave test.

level, depth averaged and vertical velocity components are then given by

$$\zeta = 4a \frac{\exp\left(-\sqrt{[3a/d^2(d+a)]}(x-ct)\right)}{\left(1+\exp\left(-\sqrt{[3a/d^2(d+a)]}(x-ct)\right)\right)^2}, \quad U = c\frac{\zeta - d}{\zeta}, \quad w = -z\frac{\partial U}{\partial x} \tag{39}$$

The solitary wave is prescribed as initial condition and the evolution in the time is computed. The wave amplitude is 2 m and the initial crest position is 80 m. The computational domain is 600 m long and the depth is 10 m. The grid size is 1 m, whereas the time step is 0.1 s. Only one layer is taken.

In Figure 6, the time series of the computed and exact water level are depicted, which demonstrates a good comparison. Figure 7 shows that the presented non-hydrostatic model conserves the shape and the amplitude of the solitary wave.

4.3. Shoaling wave over submerged bar

In this section, we focus on the performance of our non-hydrostatic solver in case of regular waves travelling over a long shore bar. Beji and Battjes [23] and Luth *et al.* [24] have performed physical tests of regular waves over a submerged trapezoidal bar in a wave flume. This flume has a length of 30 m. The still water depth is 0.4 m, which is reduced to 0.1 m at the bar. The offshore slope is $\frac{1}{20}$ and the shoreward slope is $\frac{1}{10}$. The experiments do have active wave absorption. Surface elevations are measured with wave gauges at several locations. Three measurement conditions have been considered as described by Dingemans [25]. Here, we shall consider two non-breaking situations, i.e. condition A with imposed wave period and amplitude of 2.02 s and 1.0 cm, respectively, and condition C with $T = 1.01$ s and $a = 2.05$ cm. On the analogy of Dingemans [25], the data obtained by Luth *et al.* [24] scaled to the scales of Beji and Battjes [23] are used for comparison with the numerical results obtained with the present method. The geometry as employed in the calculations is shown in Figure 8.

A large deformation of the wave occurs due to the interaction with the bar. The shoaling wave becomes non-linear through the generation of bound higher harmonics on the upward

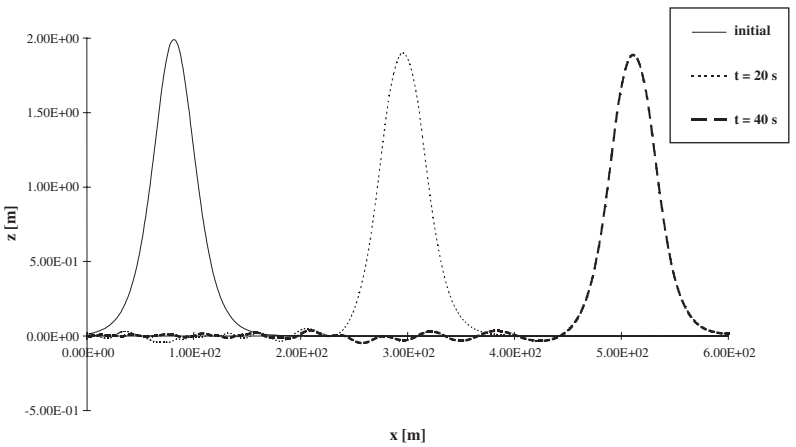

Figure 7. Computed water levels along the channel at three different time steps for the solitary wave test.

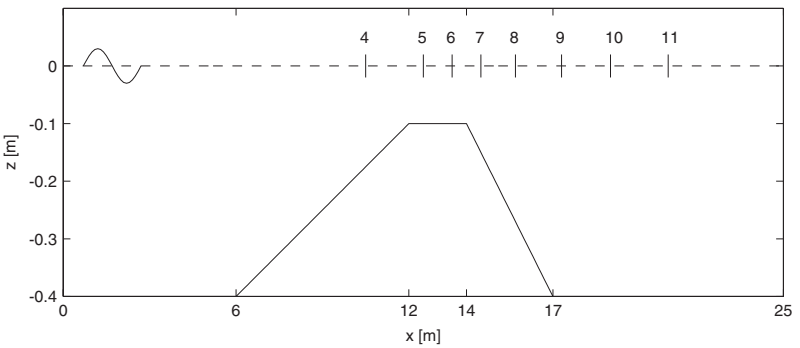

Figure 8. Bottom geometry and location of wave gauges as used in the computations.

slope of the bar and on the downward slope these harmonics become free, resulting in an irregular wave pattern. The numerical reproduction of this pattern has shown to be very demanding with respect to the accuracy of the computed dispersion frequency. For instance, Li and Fleming [12] needed 10 vertical layers in their Navier–Stokes computation, whereas Zhou and Stansby [10] and Lin and Li [13] used 21 vertical grid points. Also, Casulli [4] employed 16 vertical grid points to obtain reasonable results.

The computational domain is 35 m long of which the last 10 m consists of a sponge layer. For the simulation of both wave conditions A and C, an equidistant horizontal grid spacing of 0.0125 m is used to ensure that the free higher harmonics can be properly calculated. With respect to condition A, two calculations are carried out, namely one using a single layer and one employing two equidistant layers. In both cases, the time step is taken as $\Delta t = 0.01$ s. Concerning condition C, a computation with two equidistant layers and $\Delta t = 0.005$ s is made.

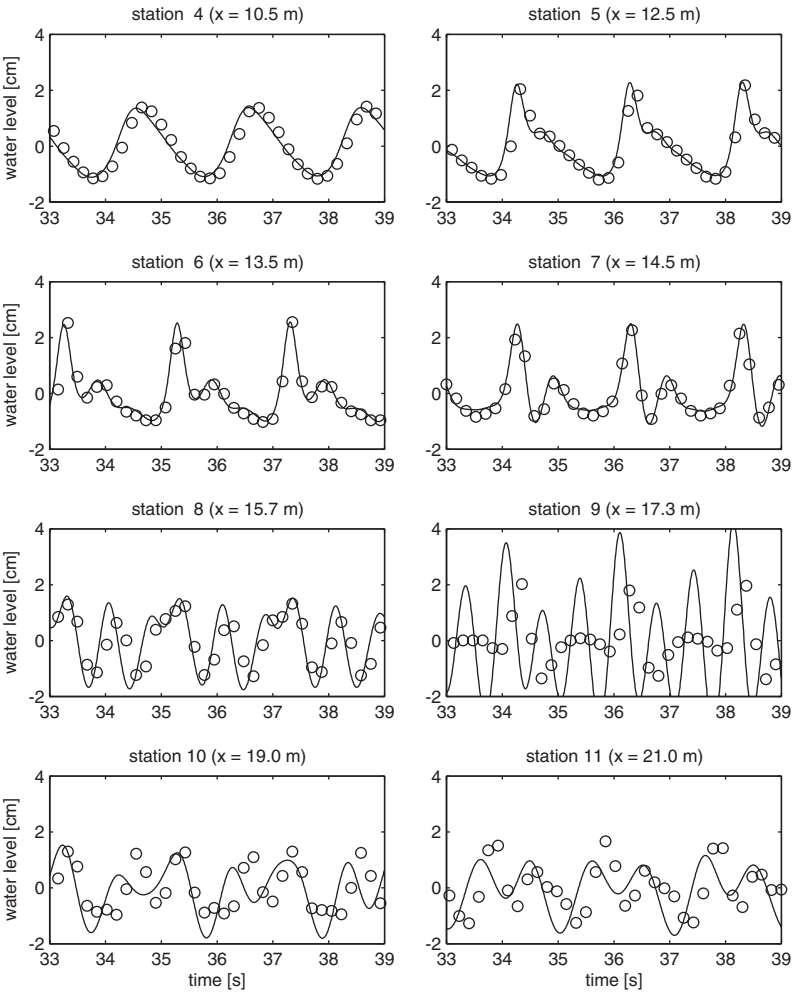

Figure 9. Computed surface elevations at several stations obtained with one layer compared to the measured ones of condition A for the wave over submerged bar. Present method (solid line), experiment (circles).

Comparisons between the measurements for wave condition A and the results of the computations using one and two layers, respectively, at eight locations are plotted in Figures 9 and 10.

Figure 9 indicates that the shoaling process on the upward slope of the bar is well described by the proposed model using a single layer. On the other hand, as expected, behind the downward slope of the bar, discrepancies between computed and measured values clearly manifest themselves. Again, these results demonstrate that the dispersion properties of the non-hydrostatic flow solver, using a single layer, are similar to the Boussinesq-like model of Peregrine [16].

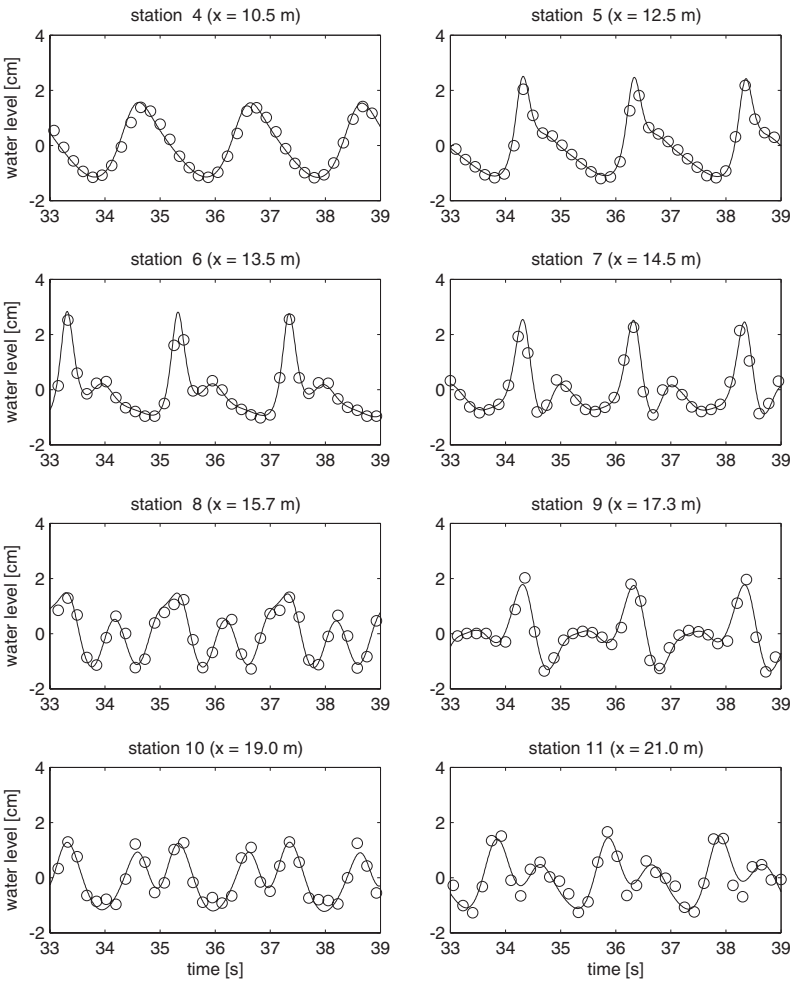

Figure 10. Computed surface elevations at several stations obtained with two layers compared to the measured ones of condition A for the wave over submerged bar. Present method (solid line), experiment (circles).

The results of the model with two layers, as presented in Figure 10, show the improved dispersion for the higher-frequency components occurring in shorter waves behind the bar. The quality of these results is comparable with the results obtained with Boussinesq-type models as presented in Reference [25].

Finally, we consider the wave condition C. For this case, we have $kH \approx 1.7$, so the basic wave is relatively short. Figure 11 displayed the comparison between numerical results obtained with two layers and measurements. Overall, the present method reproduces the experimental results for condition C considerable well. Also, to the authors' knowledge, no results obtained with a non-hydrostatic Navier–Stokes solver for this test case have been published earlier.

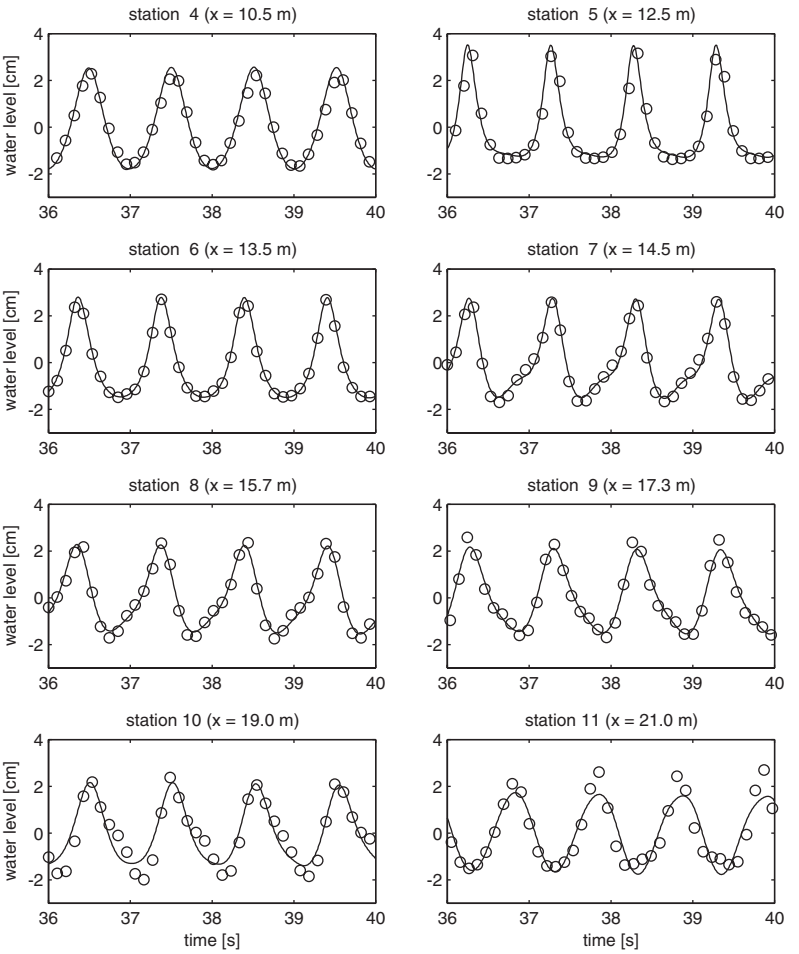

Figure 11. Computed surface elevations at several stations obtained with two layers compared to the measured ones of condition C for the wave over submerged bar. Present method (solid line), experiment (circles).

4.4. *Wave deformation by an elliptic shoal on sloped bottom*

To demonstrate the importance of wave refraction and diffraction, the present method is applied to wave propagation over an uneven bottom in a 3D configuration. We compare the numerical results with measured data from Berkhoff *et al.* [26]. They carried out a laboratory study of monochromatic wave propagation over an elliptic shoal located on a plane slope of 1/50 as shown schematically in Figure 12. Let (x', y') be the slope-oriented co-ordinates, which are related to the (x, y) co-ordinate system by means of rotation over $-20°$. The still water depth without shoal is given in meters by

$$\begin{aligned} H &= 0.45 && \text{for } y' < -5.484 \\ H &= \max(0.10, 0.45 - 0.02(5.484 + y')) && \text{for } y' \geqslant -5.484 \end{aligned} \tag{40}$$

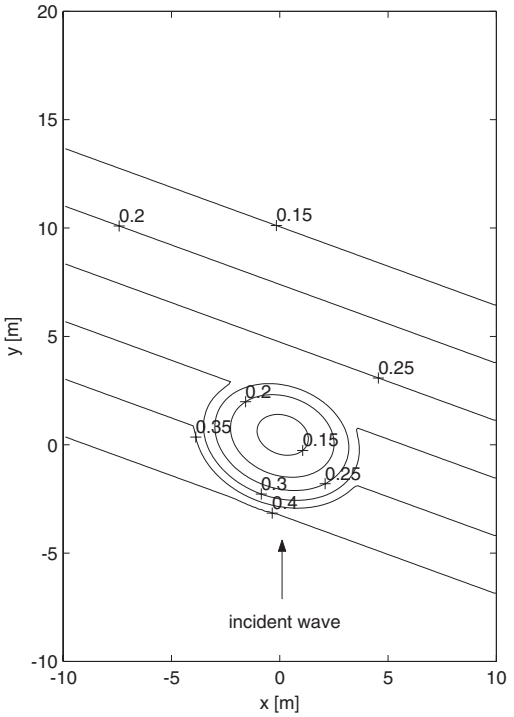

Figure 12. Bathymetry corresponding to the experiment of Berkhoff *et al.* [26].

Note that the minimum depth is set to 10 cm since, only non-breaking waves are considered in this study. The boundary of the shoal is given by

$$\left(\frac{x'}{4}\right)^2 + \left(\frac{y'}{3}\right)^2 = 1 \tag{41}$$

whereas the thickness of the shoal is

$$d = -0.3 + 0.5\sqrt{1 - \left(\frac{x'}{5}\right)^2 - \left(\frac{y'}{3.75}\right)^2} \tag{42}$$

Regular waves with frequency of 1 Hz and wave height of 4.64 cm are generated at lower boundary $y = -10$ m. At the end of the computational domain, $y = 20$ m, waves are completely absorbed by means of a sponge layer as defined by (11) with $L = 5$ m. Reflecting walls are placed on two side boundaries located at $x = -10$ and 10 m, where conditions (13) are imposed.

The grid size in both directions is set to $\Delta x = \Delta y = 0.05\ \text{m} \approx \lambda/30$, where λ denotes the wavelength in the deeper part. Since, $kH \approx 1.9$ in front of the domain, which is relatively large, only computation with two layers is carried out. Note that over the shoal shorter waves

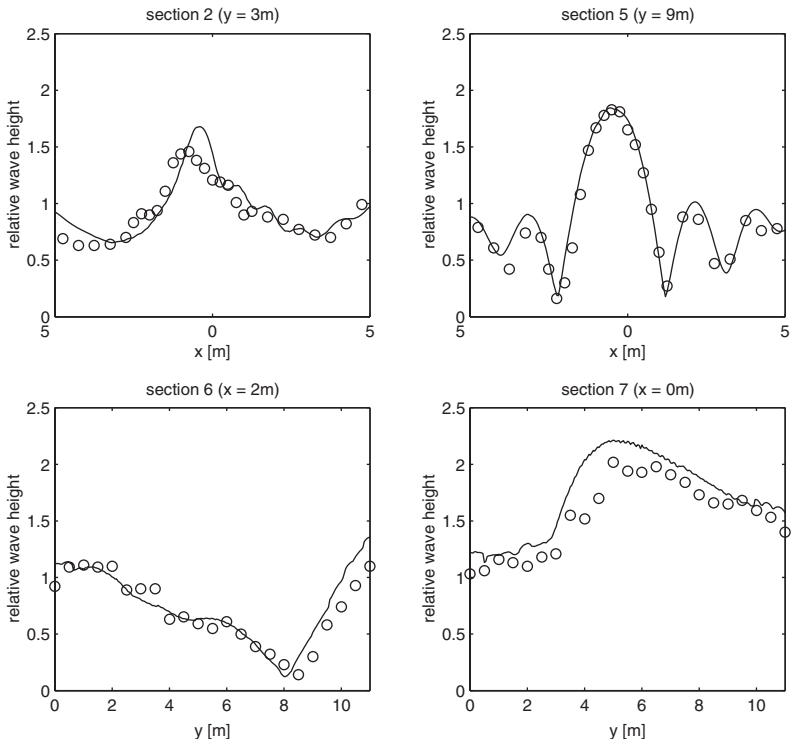

Figure 13. Computed (solid line) and measured (circles) relative wave heights along sections 2, 5–7 for the wave over elliptic shoal.

are generated. The time step is taken as 0.01 s, whereas the simulation period is set to 30 s, so that a stationary solution is obtained.

Wave heights along eight transects near the shoal were measured in the experiment. Figure 13 shows comparison of wave height relative to the incident one at four of these transects, which are the most informative ones, between the model results and the experimental data. The computed wave height is obtained by taking the difference between maximum and minimum free-surface elevation considered over a time interval in which the wave form is permanent.

Due to refraction, wave focussing occurs behind the shoal with a maximum wave height of approximately 2.2 times the incident wave height (near point $x = 0, y = 5$). The computed maximum wave height at sections 2 and 7 are slightly over predicted. On the other hand, at sections 5 and 6, the calculated minimum wave heights agree very well with the measured ones. This indicates that our model produces the significantly non-linear effects of $O(\varepsilon)$ with $\varepsilon = a/H$ very accurately. Overall, the model results are close to the experimental data. Similar results have been obtained elsewhere using a Navier–Stokes solver with 11 vertical grid points developed by Li and Fleming [12] and the extended Boussinesq-type wave model of Nwogu [2] as discussed in Reference [27].

5. CONCLUSIONS

We have presented a method that enables to calculate wave dynamics in free-surface flow effectively by means of solving the Euler or Navier–Stokes equations with a very limited number of vertical grid points. This method utilizes the Keller-box implicit scheme that approximates the non-hydrostatic vertical pressure gradients at different vertical grid points simultaneously. As a result, this technique provides a very accurate solution with optimal computational efficiency. It turns out that the quality of the results obtained with the proposed technique using a single layer is comparable with or slightly better than results published elsewhere for standard Boussinesq equations derived by Peregrine [16]. Furthermore, using two layers at least, the new method is also able to calculate the propagation of fairly short waves in relative deep water accurately and has similar linear dispersion characteristics as the extended Boussinesq-type models of Madsen en Sørensen [1] and Nwogu [2]. Based on the results demonstrated in this paper, we may conclude that the non-hydrostatic free-surface flow solver presented in this paper can capture the essential wave phenomena, such as shoaling, dispersion, refraction and diffraction.

In conclusion, it is expected that the proposed method may be computationally competitive with the extended Boussinesq-type wave models. Furthermore, it can be easily extended to include turbulence and wave breaking for the application to wave propagation in the surf zone. Also, contrary to the Boussinesq models, the present algorithm can be applied to very deep water regions. Furthermore, it is intended as the start of the development towards the modelling of interaction of waves with rotational currents. Finally, it is believed that further significant acceleration of this method in time can be realized through parallelization and domain decomposition. In this context, the method can be made more competitive with the generic shallow water solvers by means of the application of domain decomposition, in which the non-hydrostatic component of pressure need only to be calculated for subdomains where its effect is relatively important.

REFERENCES

1. Madsen PA, Sørensen OR. A new form of the Boussinesq equations with improved linear dispersion characteristics. Part A slowly-varying bathymetry. *Coastal Engineering* 1992; **18**:183–204.
2. Nwogu O. Alternative form of Boussinesq equations for nearshore wave propagation. *Journal of Waterway, Port, Coastal and Ocean Engineering* 1993; **119**:618–638.
3. Casulli V, Stelling GS. Numerical simulation of 3D quasi-hydrostatic, free-surface flows. *Journal of Hydraulic Engineering ASCE* 1998; **124**:678–686.
4. Casulli V. A semi-implicit finite difference method for non-hydrostatic, free-surface flows. *International Journal for Numerical Methods in Fluids* 1999; **30**:425–440.
5. Stelling GS, Busnelli MM. Numerical simulation of the vertical structure of discontinuous flows. *International Journal for Numerical Methods in Fluids* 2001; **37**:23–43.
6. Casulli V, Cheng RT. Semi-implicit finite difference methods for three-dimensional shallow water flow. *International Journal for Numerical Methods in Fluids* 1992; **15**:629–648.
7. Mahadevan A, Oliger J, Street R. A nonhydrostatic mesoscale ocean model. Part II: numerical implementation. *Journal of Physical Oceanography* 1996; **26**:1881–1900.
8. Mayer S, Garapon A, Sørensen LS. A fractional step method for unsteady free-surface flow with applications to non-linear wave dynamics. *International Journal for Numerical Methods in Fluids* 1998; **28**:293–315.
9. Stansby PK, Zhou JG. Shallow-water flow solver with non-hydrostatic pressure: 2D vertical plane problems. *International Journal for Numerical Methods in Fluids* 1998; **28**:541–563.
10. Zhou JG, Stansby PK. An arbitrary Lagrangian-Eulerian σ (ALES) model with non-hydrostatic pressure for shallow water flows. *Computer Methods in Applied Mechanics and Engineering* 1999; **178**:199–214.
11. Stelling GS, Van Kester JAThM. On the approximation of horizontal gradients in sigma co-ordinates for bathymetry with steep slopes. *International Journal for Numerical Methods in Fluids* 1994; **18**:915–935.

12. Li B, Fleming CA. Three-dimensional model of Navier–Stokes equations for water waves. *Journal of Waterway, Port, Coastal and Ocean Engineering* 2001; **127**:16–25.
13. Lin P, Li CW. A σ-coordinate three-dimensional numerical model for surface wave propagation. *International Journal for Numerical Methods in Fluids* 2002; **38**:1045–1068.
14. Lam DCL, Simpson RB. Centered differencing and the box scheme for diffusion convection problems. *Journal of Computational Physics* 1976; **22**:486–500.
15. Rubin SG, Khosla PK. Polynomial interpolation methods for viscous flow calculations. *Journal of Computational Physics* 1977; **24**:217–244.
16. Peregrine DH. Long waves on a beach. *Journal of Fluid Mechanics* 1967; **27**:815–827.
17. Dingemans MW. *Water Wave Propagation Over Uneven Bottoms*. World Scientific: Singapore, 1997.
18. Van der Vorst HA. Bi-CGSTAB: a fast and smoothly converging variant of Bi-CG for the solution of nonsymmetric linear systems. *SIAM Journal on Scientific and Statistical Computing* 1992; **13**:631–644.
19. Van der Vorst HA. Iterative solution methods for certain sparse linear systems with a non-symmetric matrix arising from pde-problems. *Journal of Computational Physics* 1981; **44**:1–19.
20. Chen X. Three-dimensional hydrostatic and non-hydrostatic modeling of seiching in a rectangular basin. In *Proceedings of the 6th International Conference Estuarine and Coastal Modelling*, Spaulding ML, Bulter L (eds). New Orleans, LA, 2000; 148–161.
21. Weilbeer H, Jankowski JA. A three-dimensional non-hydrostatic model for free surface flows—development, verification and limitations. In *Proceedings of the 6th International Conference Estuarine and Coastal Modelling*, Spaulding ML, Bulter L (eds). New Orleans, LA, 2000; 162–177.
22. Namin MM, Lin B, Falconer RA. An implicit numerical algorithm for solving non-hydrostatic free-surface flow problems. *International Journal for Numerical Methods in Fluids* 2001; **35**:341–356.
23. Beji S, Battjes JA. Experimental investigation of wave propagation over a bar. *Coastal Engineering* 1993; **19**:151–162.
24. Luth HR, Klopman G, Kitou N. Project 13G: Kinematics of waves breaking partially on an offshore bar; LDV measurements for waves with and without a net onshore current. *Technical Report* H1573, Delft Hydraulics, 1994.
25. Dingemans MW. Comparison of computations with Boussinesq-like models and laboratory measurements. *Technical Report* H1684.12, Delft Hydraulics, 1994.
26. Berkhoff JCW, Booy N, Radder AC. Verification of numerical wave propagation models for simple harmonic linear water waves. *Coastal Engineering* 1982; **6**:255–279.
27. Wei G, Kirby JT, Sinha A. Generation of waves in Boussinesq models using a source function method. *Coastal Engineering* 1999; **36**:271–299.

